Dynamic In Vivo Protein Carbonyl Biosensor for Measuring Oxidative Stress

Roman Kostecki[†,▽,*], Azim Arman[†,§], Bin Zhang[‡], Kai-Hung Yang[‡], Roger J. Narayan[‡], Mark R. Hutchinson[†,§], Heike Ebendorff-Heidepriem[†,▽]

[†] ARC Centre of Excellence for Nanoscale BioPhotonics (CNBP) and Institute for Photonics and Advanced Sensing (IPAS), The University of Adelaide, Adelaide, SA 5005, Australia

[▽] School of Physical Sciences, The University of Adelaide, Adelaide, South Australia 5005, Australia

[§] Adelaide Medical School, The University of Adelaide, Adelaide, South Australia 5005, Australia

[‡] Joint Department of Biomedical Engineering, University of North Carolina and North Carolina State University, Raleigh, NC, USA

KEYWORDS: Oxidative stress, Oxygen metabolism, Redox balance, Biological sensing, Optical sensing, Biosensor

ABSTRACT: Oxidative stress is intimately linked to cellular energy balance and occurs when there is an imbalance between production and accumulation of reactive oxygen species in cells and tissues and the ability of a biological system to keep in a redox steady state. While protein carbonyls are an easily detectable marker of oxygen metabolism and oxidative stress, all methods to date have required significant sample preparation and do not provide the ability to measure dynamic changes. To overcome this problem, we develop the first method for measuring in vivo concentration changes of protein carbonyls using a minimally invasive optical fiber biosensor. We use this biosensor to measure redox balance and oxidative stress within living systems by measuring dynamic in vivo concentration changes of protein carbonyls.

1. INTRODUCTION

Oxidative stress occurs when there is an imbalance between formation and regulation of reactive oxygen species (ROS) in cells and tissues, causing ROS levels to accumulate.[1] This imbalance leads to damage of important biomolecules and cells, with potential impact on the whole organism. Oxidative stress influences many physiological processes including the immune system and cellular communication,[2] and has been linked to intense exercise, inadequate diet, ageing and several age-related disorders, as well as many chronic diseases.[3-5] Some of the chronic diseases shown to be associated with increased levels of oxidative stress include; cardiovascular diseases, including vascular diseases, high cholesterol, stroke, heart failure, and hypertension;[6] cancer;[7] Parkinson's disease;[8] Alzheimer's disease;[9] diabetes;[10] kidney disease;[11] rheumatoid arthritis;[12] sepsis,[13] and; respiratory distress syndrome.[14, 15]

Protein carbonyls (aldehydes and ketones) represent a marker of overall oxygen metabolism and oxidative stress, as they are generated by multiple different reactive oxygen species in blood, tissues, and cells.[16] Protein carbonyls are abundant in plasma, chemically stable, and an easily detectable marker of oxidative stress using a wide variety of laboratory-based analytical techniques.[17] These methods for measurement of carbonyl content in biological samples were developed in the early 1970s and are still applied today. The main methods range from simple spectrophotometric analysis to liquid chromatography and mass spectrometry. All the current methods are *in vitro* and require careful sample handling and preparation and reported protein concentrations differ considerably depending on the applied protocols.[17] For example, ELISA is considered the best available method to quantify protein carbonyl concentrations, whereas immunoblotting allows comparable detection of the molecular weight of oxidized proteins.[18] These methods are widely used for the interpretation of changes in redox balance due to exercise, diabetes, cellular damage, aging, and age-related disorders.[19] While these methods for measuring protein carbonylation have been implemented in different laboratories around the world, to date no methods prevail as the most accurate, reliable, and robust.[20] All of the current methods for measuring protein carbonylation require sample preparation and yield information that is static in nature and therefore unable to measure dynamic changes in protein carbonylation. It would be far more advantageous to have a small calibrated device that can continuously monitor *in vivo* concentrations of protein carbonyls. By providing real-time critical information about oxidative stress levels, such a device could improve outcomes for people living with chronic disease and age-related disorders, as well as provide crucial redox balance information for athletes and livestock, and ultimately improve our understanding about the mechanisms affecting overall health.

Optical fiber probes offer a minimally invasive approach to creating such a device for reporting in vivo physiological signals.[21] The key benefit of optical fibers for in vivo sensing are their small size and their inert glass composition, allowing for minimally invasive implantation, and non-destructive probing deep within tissue. They make it possible to reduce the sensing area down to hundreds or tens of microns, so that

molecular information on a local scale can be obtained, and yet with a signal to noise ratio sufficient to capture specific rare and rapid molecular events.[22] Critically, such light-based sensing technologies lend themselves to the repeated measurement of in vivo molecular events. The molecular specificity in these approaches is derived from recognition molecules, such as chemosensor fluorophores that specifically target chosen analytes.[23] Fluorescence is highly compatible with optical fibers as a sensing modality since the chemosensors can be attached either along the length or at the tip of the fiber surface.[24] The chemosensors can then be excited by the light guided along the fiber and the resulting fluorescence signal is collected via the same fiber. Optical fiber-based biosensors have been shown to detect a wide range of biologically relevant molecules such as viruses, toxins, drugs, antibodies, tumor biomarkers and tumor cells glucose and a wide range of biochemicals.[25] Different strategies have been used to functionalize fiber cores with chemosensors, such as covalently attaching silanes, physical attachment of charged polymers (polyelectrolytes), thin-film deposition of doped polymers, or introducing functional groups on the fiber surface with surface linking chemistry.[26]

Here we present initial results of an optical fiber biosensor device, made by combining 3D printed needle technology with an optical fiber tip sensor, to produce an optical fiber-based reversible protein carbonylation biosensor capable of providing *in vivo* information about dynamic changes in oxidative stress levels and redox balance.

2. EXPERIMENTAL SECTION

2.1 Fiber Tip Sensor. 4 mg of fluorescein-5-thiosemicarbazide (Cayman Chemical; FTSC) was added to 0.5 ml e-shell 300 acrylate-based photopolymer (EnvisionTEC). This photopolymer is Class-IIa biocompatible. FTSC is known to reversibly bind to protein carbonyls and induce fluorescence (495 / 517 nm Ex. / Em. Max). The mixture was vortexed for one minute then sonicated for ten minutes then vortexed for a further one minute. A 600 µm patch fiber (Thorlabs; M29L05) was cut in half and stripped back to expose the solid glass core, which was then cleaved. The tip of the glass core was functionalized by dipping the tip into the FTSC doped photopolymer for 1 second. The FTSC doped photopolymer left behind at the fiber tip was then exposed to 488 nm laser light (Integrated Optics MatchBox CW) at 142 µW by coupling into the light into fiber via the SMA connector for thirty seconds. Next, the tip of the fiber was dip cleaned by quickly dipping into a solution of 50/50 ratio acetone and isopropanol (IPA) followed by quickly dipping into a solution of only IPA. The last step of the procedure was to expose the fiber tip to 80 mW of 405 nm laser light (Integrated Optics MatchBox CW) by coupling the light into the SMA connector for 5 minutes. This procedure left behind a layer of FTSC doped polymer at tens of micrometers thick on the tip of the cleaved M29L05 patch fiber to create a fiber tip oxidative stress sensor (tip sensor).

2.2 Measurement Setup. As illustrated in Figure 1, the fully fiber coupled setup is comprised of a 488 nm laser light source (Integrated Optics MatchBox CW) and shutter to send a 0.1 sec pulse of 130 µW excitation light to the tip sensor via a bifurcated fiber bundle (Thorlabs; RP21). The back-reflected signal was coupled back into the bifurcated fiber bundle, passed through a 488 nm long-pass edge filter (Semrock; BLP01-488R-25), and characterized using an Ocean Optics QE Pro spectrometer.

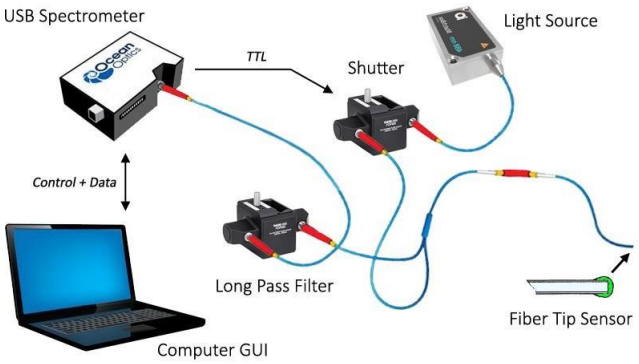

Figure 1: Schematic of the measurement setup.

2.3 *β*-hydroxybutyrate (BHB) characterization solutions. A 0.5 mM BHB stock solution was prepared by reconstituting the contents of a β-hydroxybutyrate Standard vial (Cayman Chemical Company; 700192), which contains a lyophilized powder of DL-hydroxybutyrate, with 2 ml of β-Hydroxybutyrate Assay Buffer (Cayman Chemical Company; 700191). The reconstituted solution is stable for six hours on ice. The standard curve was obtained immediately by using the setup to measure the stock solution and then reducing concentrations of the BHB solution. These reducing concentrations were prepared by adding an additional appropriate volume of β-Hydroxybutyrate Assay Buffer to the 0.5 mM BHB stock solution to obtain a stepwise change in concentration, as shown in Table 1.

Table 1: BHB solution preparation.

Concentration	Buffer Added	Total Volume
0.5 mM	-	200 µl
0.4 mM	50 µl	250 µl
0.3 mM	83 µl	333 µl
0.2 mM	167 µl	500 µl
0.1 mM	500 µl	1000 µl

2.4 3D Printed Needles. The hollow microneedles were designed using Solid-works software, and the bore sizes of microneedles were determined based on the diameters of the fiber tip sensor and capillary. The predesigned hollow microneedles were produced from Class-IIa biocompatible e-shell 300 acrylate-based photopolymer (EnvisionTEC) using an Envisiontec Perfactory stereolithography machine. The needle

design is shown in Figure 2(a); the final 3D printed microneedle is shown in Figure 2(b).

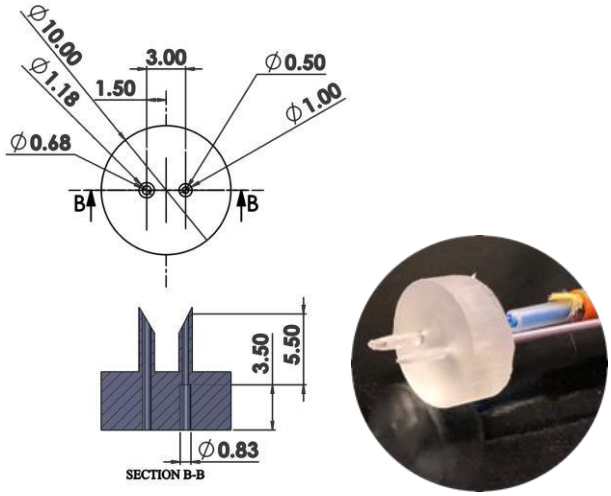

(a) (b)

Figure 2: (a) Needle design schematic, and (b) 3D printed needle fitted with 600 µm optical fiber tip sensor and 500 µm capillary.

2.6 *In-vivo* Live Mouse Measurements.

Subjects: Adult male Balb/c mice were supplied from the Animal Resources Centre (Murdoch, WA, Australia) housed in 18°C ± 6 with 12:12 hours light: dark and with food and water provided ad libitum. All procedures were conducted under the University of Adelaide Animal Ethics approval number M-2018-024 in compliance with the Australian code for the care and use of animals for scientific purposes.

Surgical procedure: Under deep anaesthesia with 2% inhalation isoflurane and animal in ventral recumbency, the lower thigh area was prepared aseptically for an unrelated surgical procedure. A subcutaneous pocket was created via an 18-gauge needle insertion in the semitendinosus muscle. Next, the tip sensor was implanted in the muscle mass via the inserted needle for the duration of the experiment. To induce hypoxia, the inhalation isoflurane was increased to 5% and the oxygen level was reduced to aminimal level; protein carbonyl sensing continued for the remainder of the experiment until the time of death. The same procedure was done in subcutaneous lumbar area.

3. RESULTS AND DISCUSSION

3.1 Sensor Characterization. No fluorescence was observed when the tip sensor was placed in water only. However, intense fluorescence with a peak at 517 nm formed within two minutes of placing the tip sensor in a 0.5 mM concentration of BHB, as shown in Figure 3.

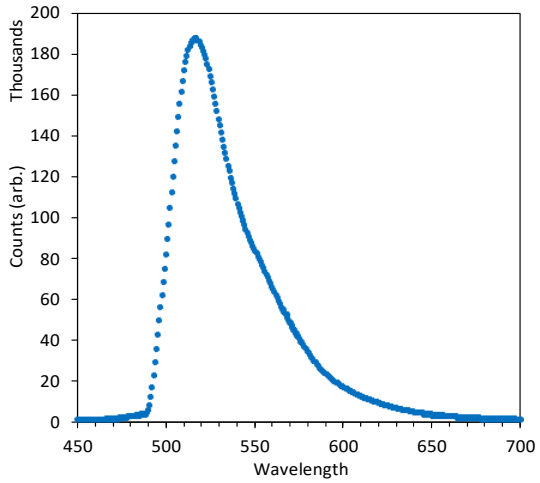

Figure 3: Typical spectrum measured from the tip sensor in 0.5 mM solution of BHB.

To test the stability and reversibility of the tip sensor while obtaining a standard curve, measurements were performed every minute over a one-hour period using decreasing concentrations of the BHB stock solutions described in Sec. 2.3. The intensity of the fluorescence peak at 517 nm was found to be proportional to the concentration of BHB following the equation of $S = 27174223 \cdot C$; where S is the intensity in counts and C is the Molar concentration. This linear dependence is shown by the red dotted line in Figure 4, along with the unadjusted peak counts measured from one pulse every minute with the sensor in the BHB stock solutions with decreasing concentrations every 10 minutes. The last measurement was performed in buffer only. The tip sensor was further characterized in a mouse embryo cell growth assay to ensure its biological compatibility, which showed no affects to the viability and growth of the cell culture (mouse embryo assay).

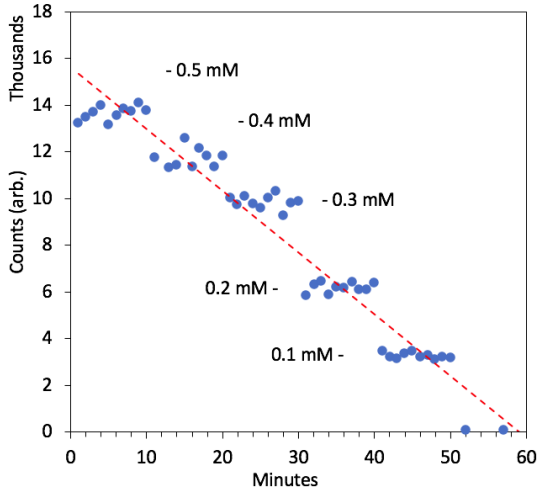

Figure 4: Response of tip sensor with decreasing concentrations of BHB every ten minutes. The peak values of measurements recorded every minute are shown along with the fitted linear regression indicated by the red dotted line.

3.2 *In vivo* porcine skin measurements. Fresh porcine skin was used to further characterize the tip sensor. To achieve this, the tip sensor with microneedles shown in Section 2.4 was used for subcutaneous measurement. A microneedle length of 5 mm was chosen so that the tip of the needles would penetrate the epidermis and dermis layers of the porcine skin to locate within the subcutaneous tissues.[27, 28] The microneedle array consisted of two needles, one of which was used for the fiber tip sensor and the other needle contained a capillary so that sample analyte or medications could be injected alongside the sensor. The microneedle was inserted into three different locations of fresh (three hours old) porcine skin obtained from an abattoir on the morning before the experiment; measurements were performed every minute. Results from the tip sensor, shown in Figure 5, indicated that the protein carbonyl concentrations were significantly different at these three locations, with an increased concentration detected where there was no blood in the sample.

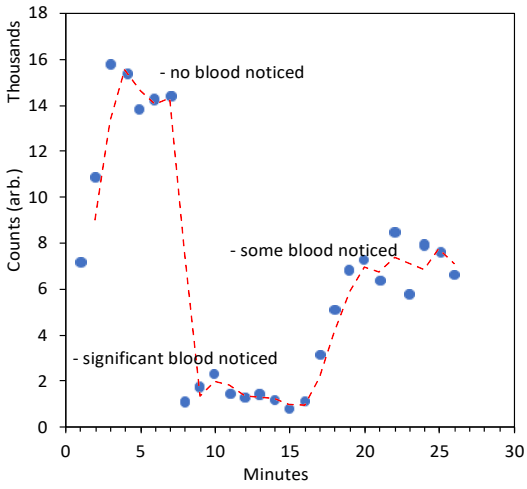

Figure 5: Response from 3D printed needle fitted with tip sensor in three locations of porcine skin. The peak values at 517 nm of measurements recorded every minute are shown.

The signal was an order of magnitude higher in regions of the skin where blood was not noticeably present. One possible explanation for this is that protein carbonyl levels formed earlier in response to oxidative stress could be more stable in subcutaneous tissue compared to blood. The same experiment was repeated on nine-day old porcine skin, where the biosensor showed very low intensity; orders of magnitude less signal compared to the three hours old sample. The results also show that it took around two minutes for the tip sensor to respond to changes in concentration of protein carbonyls, each time the tip sensor was inserted into the porcine skin.

3.3 Subcutaneous tissue diffusion measurements. The efficient application of subcutaneous injection of drug solution relies on a detailed understanding of the mass transport of the drug substance in surrounding biological tissues upon release. Experimental techniques capable of characterizing these drug transport processes in vivo are highly needed in the design and development of controlled release drug delivery systems. The microneedle array was designed with a 3 mm gap between the capillary injection needle and the tip sensor needle to measure the dynamic concentration flux dynamics within the subcutaneous tissue. These types of measurements can help with understanding the mechanical and diffusion properties of subcutaneous tissue with the potential to avoid adverse effects of subcutaneous drug delivery treatments. The measurements were achieved by inserting the microneedle array into 10 days old porcine skin and taking measurements every minute from the tip sensor within the microneedle array while pumping (LongerPump BT100-1F) BHB at a controlled flow rate through the capillary side of the microneedle array. For the first forty minutes a 5 µL/min flow rate of 1 mM BHB solution was applied to the capillary side of the microneedle array. The intensity of the fluorescence peak at 517 nm from the tip sensor steadily increased with a slight bell curve to a maximum 16 thousand counts, as shown in Figure 6. Next, the tip sensor was removed and reinserted into a fresh part of the porcine skin sample and a 20 µL/min flow rate of 0.5 mM BHB solution was applied for the next thirty-five minutes to the capillary side of the microneedle array. The intensity of the tip sensor initially reduced to around three thousand counts and then steadily increased to around eight thousand counts with a well-defined bell curve shape. Finally, the tip sensor was again removed and reinserted into a fresh part of the porcine skin sample and a 5 µL/min flow rate of 0.5 mM BHB solution was applied for the next 50 minutes to the capillary side of the microneedle array. The intensity of the tip sensor again initially reduced to around three thousand counts and then steadily increased to around 7 thousand counts with a well-defined bell curve. The rise time of the tip sensor response to the 5 µL/min flow rate was slower compared with the rise time of the 20 µL/min flow rate, at the same concentration of 0.5 mM BHB. The starting point for all these measurements was approximately one thousand counts, which is expected to be because of the residual concentration of protein carbonyls in the subcutaneous tissue.

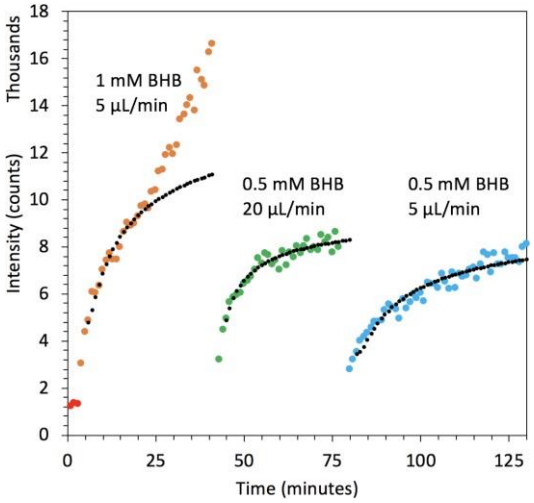

Figure 6: Response of tip sensor at three different locations and varying conditions (flow rate and concentration) within the subcutaneous space of several day old porcine skin.

Diffusion in the subcutaneous tissue is modelled by Fick's law[29], which in one dimension can be described by:

$$\frac{\partial C}{\partial t} = D\frac{\partial^2 C}{\partial x^2} \quad (1)$$

were x is the distance, t is the time, C refers to the concentration of the injected analyte, and D is the analyte diffusivity through the subcutaneous tissue (diffusion coefficient). D is assumed to be constant in the concentration range investigated. We have the boundary conditions that at $t = 0, x = 0$ and $C = C_0$. Using the infinite approximation, a solution of Equation (1) is:[29]

$$C(x,t) = \frac{C_0}{2} - \frac{C_0}{\sqrt{\pi}}\int_0^{\frac{x}{2\sqrt{Dt}}} e^{-t^2} dt \quad (2)$$

The right side of Equation (2) is the familiar error function which can be integrated using a power series expansion. Using the first two terms of the power series expansion as a quick approximation with the assumptions that $x > 0$ and relatively small, $t > 0$ and relatively large, Equation (2) becomes:

$$C(x,t) = C_0\left(\frac{1}{2} - \frac{12Dtx - x^3}{24Dt\sqrt{Dt\pi}}\right) \quad (3)$$

Equation (3) was fitted to the data shown in Figure 6 to determine the diffusion coefficient D, as shown by the narrow dark results for each experiment. While Equation (3) fitted well to both 0.5 mM results, the 1 mM results deviated from the expected error function curve which might be due to leakage or backflow during the experiment. However, the model did fit very well ($R^2 = 0.952$) to the first twenty-two minutes of the 1 mM experiment. The results of the fitting indicate that $D = 1.5 \times 10^{-8}$ at a flow rate of 5 µL/min, as shown by 1 mM and 0.5 mM results. At a flow rate of 20 µL/min, D increased by more than twice to 3.7×10^{-8}. In the future, it might be useful to perform a more extensive set of experiments that include a larger set of flow rates and concentrations to better understand how the diffusion coefficient of subcutaneous tissue varies with flow.

Table 2: Results of Equation 3 fitted to data in Figure 6.

Concentration BHB	Flow Rate (µL/min)	D (m^2/s)	R-square
1 mM	5	1.5×10^{-8}	0.952
0.5 mM	20	3.7×10^{-8}	0.9151
0.5 mM	5	1.5×10^{-8}	0.9153

3.4 *In vivo* mouse measurements. Next, the biosensor was used to measure protein carbonylation levels in an anesthetized live mouse (as described in Section 2.6). In this case, the polymer microneedle was replaced by a stainless-steel hypodermic needle. The tip sensor was placed in the subcutaneous space under the skin via the hypodermic needle for the first twelve minutes and then placed in the hind leg muscle for the remaining ten minutes. The results revealed a detectable and relatively steady concentration of the analyte in the subcutaneous space under the skin, as shown in Figure 7. In the hind limb muscle, where there was blood, the levels were much higher and seemed to increase over the ten minutes of measurement. While an increased level was expected in the hind leg muscle[17] and considering this is the first time such a measurement was made on a living model; more work is needed to understand why the biosensor in the hind leg muscle measured an order of magnitude higher signal compared with subcutaneous measurements from the mouse or pig skin.

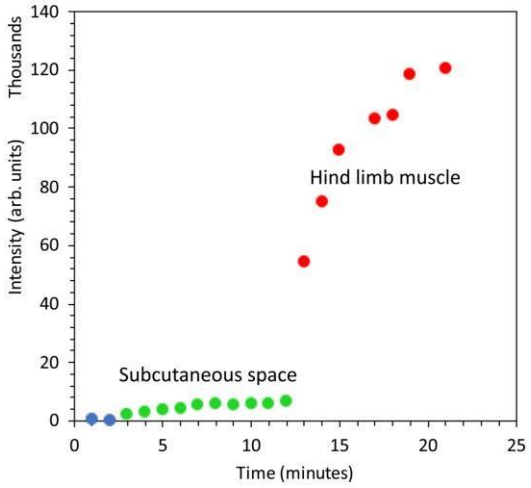

Figure 7: In vivo protein carbonylation levels in an anesthetized live mouse. The first twelve minutes were measured in the subcutaneous space and then the remaining 10 minutes were measured in the hind leg muscle.

The protein carbonyl levels were measured in the subcutaneous space under the skin of another two mice. This time the experiment was extended to one hour. As was the case for the first mouse, the result from the sensor in the second mouse also increased for the first few minutes after insertion. However, the measurement then decreased back to a relatively steady state after 20 minutes, as shown in Figure 8. Using the concentration equation discussed in Section 3.1, we find that the concentration of protein carbonyls becomes steady at around 36.8 µM. It is expected that this initial increase is due to immune response from inserting the needle and sensor, and that response quickly subsides as the sensor is left in place. This was also the steady state protein carbonyl concentration of the third mouse after 20 minutes. Unexpectedly, the third mouse did not have the same

initial increase as measured from the first two mice, as shown in Figure 8.

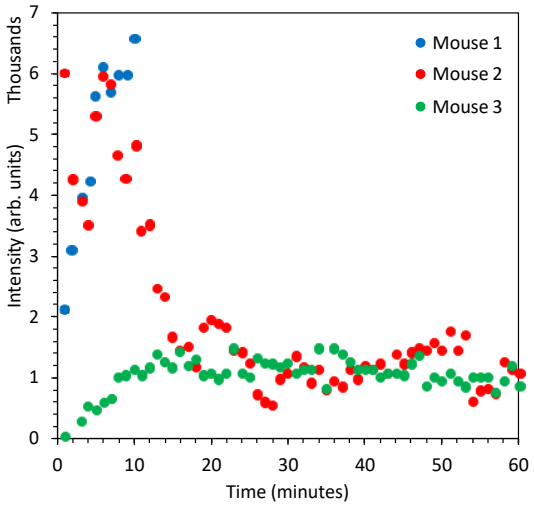

Figure 8: Protein carbonyl levels measured in the subcutaneous space of three mice for one hour.

4. CONCLUSIONS

This paper describes a new method for measuring *in vivo* dynamic protein carbonylation and initial results of those measurements. Using the small calibrated optical sensor has made dynamic measurements possible for the first time, which is far more advantageous than *in vitro* measurement requiring sample preparation. This new sensing technology has the potential to provide critical information about oxidative stress levels, which could improve outcomes for people living with chronic disease and age-related disorders, as well as provide crucial redox balance information for athletes and livestock, and ultimately improve our understanding about the mechanisms affecting overall health.

AUTHOR INFORMATION

Corresponding Author

* roman.kostecki@adelaide.edu.au

ACKNOWLEDGMENT

This work was performed in part at the OptoFab node of the Australian National Fabrication Facility utilizing Commonwealth and South Australian State Government funding and was supported by Australian Research Council (ARC) Centre of Excellence for Nanoscale Biophotonics (CE14010003). Roman Kostecki and Roger Narayan acknowledge support from NC State Starter Grants for Research Collaboration. Bin Zhang acknowledges support from the U.S . National Academy of Engineering Vest Scholars program.

REFERENCES

1. Zorov, D. B.; Juhaszova, M.; Sollott, S. J. Mitochondrial Reactive Oxygen Species (ROS) and ROS-Induced ROS Release. *Physiol. Rev.* 2014, 94, 909-950.
2. Reuter, S.; Gupta, S. C.; Chaturvedi, M. M.; Aggarwal, B. B. Oxidative stress, inflammation, and cancer: How are they linked? *Free Radic. Biol. Med.* 2010, 49, 1603-1616.
3. Lobo, V.; Patil, A.; Phatak, A.; Chandra, N. Free radicals, antioxidants and functional foods: Impact on human health. *Pharmacogn. Rev.* 2010, 4, 118-126.
4. Liguori, I.; Russo, G.; Curcio, F.; Bulli, G.; Aran, L.; Della-Morte, D.; Gargiulo, G.; Testa, G.; Cacciatore, F.; Bonaduce, D.; Abete, P. Oxidative stress, aging, and diseases. *Clin. Interv. Aging.* 2018, 13, 757-772.
5. Simioni, C.; Zauli, G.; Martelli, A. M.; Vitale, M.; Sacchetti, G.; Gonelli, A.; Neri, L. M. Oxidative stress: role of physical exercise and antioxidant nutraceuticals in adulthood and aging. *Oncotarget.* 2018, 9, 17181-17198.
6. Madamanchi Nageswara, R.; Vendrov, A.; Runge Marschall, S. Oxidative Stress and Vascular Disease. *Arterioscler. Thromb. Vasc. Biol.* 2005, 25, 29-38.
7. Sosa, V.; Moliné, T.; Somoza, R.; Paciucci, R.; Kondoh, H.; Lleonart, M. E. Oxidative stress and cancer: An overview. *Ageing Res. Rev.* 2013, 12, 376-390.
8. Wei, Z.; Li, X.; Li, X.; Liu, Q.; Cheng, Y. Oxidative Stress in Parkinson's Disease: A Systematic Review and Meta-Analysis. *Front. Mol. Neurosci.* 2018, 11, 236-236.
9. Huang, W.-J.; Zhang, X.; Chen, W.-W. Role of oxidative stress in Alzheimer's disease. *Biomed. Rep.* 2016, 4, 519-522.
10. Asmat, U.; Abad, K.; Ismail, K. Diabetes mellitus and oxidative stress-A concise review. *Saudi Pharm. J.* 2016, 24,547-553.
11. Daenen, K.; Andries, A.; Mekahli, D.; Van Schepdael, A.; Jouret, F.; Bammens, B. Oxidative stress in chronic kidney disease. *Pediatr. Nephrol.* 2019, 34, 975-991.
12. Quiñonez-Flores, C. M.; González-Chávez, S. A.; Del Río Nájera, D.; Pacheco-Tena, C. Oxidative Stress Relevance in the Pathogenesis of the Rheumatoid Arthritis: A Systematic Review. *Biomed. Res. Int.* 2016, 2016, 6097417-6097417.
13. Mantzarlis, K.; Tsolaki, V.; Zakynthinos, E. Role of Oxidative Stress and Mitochondrial Dysfunction in Sepsis and Potential Therapies. *Oxid. Med. Cell. Longev.* 2017, 2017, 5985209-5985209.
14. Brigham, K. L. Oxidant stress and adult respiratory distress syndrome. *Eur. Respir. J. Suppl.* 1990, 11, 482s-484s.
15. Marseglia, L.; D'Angelo, G.; Granese, R.; Falsaperla, R.; Reiter, R. J.; Corsello, G.; Gitto, E. Role of oxidative stress in neonatal respiratory distress syndrome. *Free Radic. Biol. Med.* 2019.
16. Frijhoff, J.; Winyard, P. G.; Zarkovic, N.; Davies, S. S.; Stocker, R.; Cheng, D.; Knight, A. R.; Taylor, E. L.; Oettrich, J.; Ruskovska, T.; Gasparovic, A. C.; Cuadrado, A.; Weber, D.; Poulsen, H. E.; Grune, T.; Schmidt, H. H. H. W.; Ghezzi, P. Clinical Relevance of Biomarkers of Oxidative Stress. *Antioxid. Redox. Signal.* 2015, 23, 1144-1170.
17. Weber, D.; Davies, M. J.; Grune, T. Determination of protein carbonyls in plasma, cell extracts, tissue homogenates, isolated proteins: Focus on sample preparation and derivatization conditions. *Redox Biol.* 2015, 5, 367-380.
18. Augustyniak, E.; Adam, A.; Wojdyla, K.; Rogowska-Wrzesinska, A.; Willetts, R.; Korkmaz, A.; Atalay, M.; Weber, D.; Grune, T.; Borsa, C.; Gradinaru, D.; Chand Bollineni, R.; Fedorova, M.; Griffiths, H. R. Validation of protein carbonyl measurement: a multi-centre study. *Redox Biol.* 2014, 4, 149-157.
19. Gonos, E. S.; Kapetanou, M.; Sereikaite, J.; Bartosz, G.; Naparło, K.; Grzesik, M.; Sadowska-Bartosz, I. Origin and pathophysiology of protein carbonylation, nitration and chlorination in age-related brain diseases and aging. *Aging (Albany NY)* 2018, 10, 868-901.

20. Rogowska-Wrzesinska, A.; Wojdyla, K.; Nedić, O.; Baron, C. P.; Griffiths, H. R. Analysis of protein carbonylation — pitfalls and promise in commonly used methods. *Free Radic. Res.* 2014, 48, 1145-1162.

21. Li, J.; Ebendorff-Heidepriem, H.; Gibson, B. C.; Greentree, A. D.; Hutchinson, M. R.; Jia, P.; Kostecki, R.; Liu, G.; Orth, A.; Ploschner, M.; Schartner, E. P.; Warren-Smith, S. C.; Zhang, K.; Tsiminis, G.; Goldys, E. M. Perspective: Biomedical sensing and imaging with optical fibers—Innovation through convergence of science disciplines. *APL Photonics* 2018, 3, 100902.

22. Kostecki, R.; Heng, S.; Mak, A. M.; Ebendorff-Heidepriem, H.; Monro, T. M.; Abell, A. D. Control of Molecular Recognition via Modulation of the Nanoenvironment. *ACS Appl. Mater. Interfaces* 2018, 10, 41866-41870.

23. Heng, S.; Nguyen, M.-C.; Kostecki, R.; Monro, T. M.; Abell, A. D. Nanoliter-scale, regenerable ion sensor: sensing with a surface functionalized microstructured optical fibre. *RSC Adv.* 2013, 3, 8308-8317.

24. Kostecki, R.; Ebendorff-Heidepriem, H.; Afshar V, S.; McAdam, G.; Davis, C.; Monro, T. M. Novel polymer functionalization method for exposed-core optical fiber. *Opt. Mater. Express* 2014, 4, 1515-1525.

25. Bosch, E. M.; Sánchez, J. A.; Rojas, S. F.; Ojeda, B. C. Recent Development in Optical Fiber Biosensors. *Sensors* 2007, 7.

26. Bachhuka, A.; Heng, S.; Vasilev, K.; Kostecki, R.; Abell, A.; Ebendorff-Heidepriem, H. Surface Functionalization of Exposed Core Glass Optical Fiber for Metal Ion Sensing. *Sensors* 2019, 19.

27. Turner, N. J.; Pezzone, D.; Badylak, S. F. Regional Variations in the Histology of Porcine Skin. *Tissue Eng. Part C Methods* 2015, 21, 373-384.

28. Lonergan, S. M.; Topel, D. G.; Marple, D. N. Chapter 5 - Fat and fat cells in domestic animals. In *The Science of Animal Growth and Meat Technology (Second Edition)*, Lonergan, S. M.; Topel, D. G.; Marple, D. N., Eds. Academic Press: 2019; pp 51-69.

29. Crank, J. *The Mathematics of Diffusion*. Oxford University Press: 1979.